$Mg(OH)_2-WS_2$ van der Waals heterobilayer: Electric field tunable band-gap crossover

M. Yagmurcukardes,[1,*] E. Torun,[2] R. T. Senger,[1] F. M. Peeters,[2] and H. Sahin[2,3,†]
[1]*Department of Physics, Izmir Institute of Technology, 35430 Izmir, Turkey*
[2]*Department of Physics, University of Antwerp, Groenenborgerlaan 171, B-2020 Antwerp, Belgium*
[3]*Department of Photonics, Izmir Institute of Technology, 35430 Izmir, Turkey*
(Received 10 March 2016; revised manuscript received 12 May 2016; published 3 November 2016)

Magnesium hydroxide [$Mg(OH)_2$] has a layered brucitelike structure in its bulk form and was recently isolated as a new member of two-dimensional monolayer materials. We investigated the electronic and optical properties of monolayer crystals of $Mg(OH)_2$ and WS_2 and their possible heterobilayer structure by means of first-principles calculations. It was found that both monolayers of $Mg(OH)_2$ and WS_2 are direct-gap semiconductors and these two monolayers form a typical van der Waals heterostructure with a weak interlayer interaction and a type-II band alignment with a staggered gap that spatially separates electrons and holes. We also showed that an out-of-plane electric field induces a transition from a staggered to a straddling-type heterojunction. Moreover, by solving the Bethe-Salpeter equation on top of single-shot G_0W_0 calculations, we show that the low-energy spectrum of the heterobilayer is dominated by the intralyer excitons of the WS_2 monolayer. Because of the staggered interfacial gap and the field-tunable energy-band structure, the $Mg(OH)_2-WS_2$ heterobilayer can become an important candidate for various optoelectronic device applications in nanoscale.

DOI: 10.1103/PhysRevB.94.195403

I. INTRODUCTION

Over the past decade, graphene, a two-dimensional (2D) form of carbon atoms arranged in a honeycomb structure, led to an enormous interest in the field of two-dimensional materials due to its exceptional physical properties [1,2]. However, the lack of a band gap is a major obstacle for the use of graphene in optoelectronic applications. Subsequently other novel 2D materials such as hexagonal structures of III-V binary compounds [3,4] and transition-metal dichalcogenides (TMDs) [5,6] have gained a lot of interest due to their wide range of band-gap energies. The synthesized members of TMDs, notably, MoS_2 [7], $MoSe_2$ [8], WS_2 [9], and recently, ReS_2 [10] and $ReSe_2$ [11], which have band gaps around 1–2 eV, are suitable monolayer materials for many optoelectronic applications [12]. Beyond being novel atomic-thick materials, lateral and vertical heterostructures of these monolayer crystals have also received considerable attention.

As constituents of possible heterostructures, TMDs are very promising. Those new members of 2D monolayer materials have tunable electronic properties from metallic to wide-gap semiconducting [13,14] and excellent mechanical properties [15]. Moreover, TMDs can be used in various fields, such as nanoelectronics [7,16,17], photonics [18–20], and for transistors [6], catalysis [21], hydrogen storage [22], and Li-ion battery applications [23]. Among TMDs, WS_2 has been studied intensively. It is an indirect-gap semiconductor in its bulk form, while it shows a transition to direct-gap character in its monolayer form [24–26]. It was shown by Ramasubramaniam that the optoelectronic properties of WS_2 and MoX_2 (X=S or Se) monolayers are tunable through quantum confinement of carriers within the monolayers [27]. Shi *et al.* showed that the electron effective mass decreases as the applied strain increases, and monolayer WS_2 possesses the lightest charge carriers among the TMDs [28]. In addition, strong excitonic features of WS_2, including neutral and redshifted charged excitons, were observed by Mak *et al.* [29]. Due to these interesting electronic and optical properties, one may go a step further and construct 2D heterostructures incorporating monolayer WS_2 with another 2D monolayer with the potential to achieve enhanced functionalities.

Recently synthesized monolayers of $Mg(OH)_2$, a member of alkaline-earth hydroxides (AEH) with formula $X(OH)_2$, where X = Mg or Ca, were studied as candidate materials for constructing such heterostructures. Magnesium and calcium hydroxides are multifunctional materials which have many important applications in industry, technology, solid-state electronics, and in photovoltaic devices [30–32]. Recently, we studied $Ca(OH)_2$ monolayer crystals and found that the number of layers of $Ca(OH)_2$ does not affect the electronic, structural, and magnetic properties qualitatively, while the intrinsic mechanical stiffness of each layer becomes slightly larger as the structure changes from monolayer to bilayer. Very recently, Torun *et al.* [33] investigated the electronic and optical properties of the heterobilayer structure GaS-$Ca(OH)_2$ and found that it is a type-II heterojunction where spatially separated charge carriers can be formed. The optical spectra of different stacking types exhibit distinct properties. Like $Ca(OH)_2$, $Mg(OH)_2$ has a layered structure in its bulk form, possessing the trigonal symmetry of the space group $P\bar{3}m1$ (brucite) [34–36]. $Mg(OH)_2$ itself is a wide-gap insulator with a band gap of 7.6 eV found experimentally for the bulk structure [37]. Chiba *et al.* reported properties of C-doped $Mg(OH)_2$ films and found that the material becomes transparent in the visible region and electrically conducting, which are favorable properties for applications in photovoltaic devices [38]. Huang *et al.* [39] found experimentally a spectral peak near the band edge corresponding to strongly localized excitons with an exciton binding energy of 0.53 eV. This indicates a strong localization of the hole and electron to the oxygen p_x and p_y states. Most recently, successful synthesis

*mehmetyagmurcukardes@iyte.edu.tr
†hasansahin@iyte.edu.tr

of $Mg(OH)_2$ monolayers on MoS_2 and their optical properties were reported by Suslu *et al.* [40]

Here we predict an electric field dependence of the electronic and optical properties of the $Mg(OH)_2-WS_2$ heterobilayer structure. Our results reveal that monolayer crystal of $Mg(OH)_2$ combined with TMDs may lead to the emergence of novel multifunctional nanoscale optoelectronic devices.

The paper is organized as follows: Details of the computational methodology are given in Sec. II. Structural and electronic properties of monolayers of $Mg(OH)_2$ and WS_2 are presented in Sec. III, while the structural properties of the $Mg(OH)_2-WS_2$ heterobilayer are presented in Sec. IV. The effect of an external electric field on the electronic properties of the heterobilayer structure is given in Sec. V. In Sec. VI the electric field dependence of the optical properties of the heterobilayer are discussed. Finally, we conclude in Sec. VII.

II. COMPUTATIONAL METHODOLOGY

For our first-principles calculations, we employed the plane-wave basis projector augmented wave (PAW) method in the framework of density-functional theory (DFT). For the exchange-correlation potential, the generalized gradient approximation (GGA) in the Perdew-Burke-Ernzerhof (PBE) form [41,42] was employed as implemented in the Vienna *Ab Initio* Simulation Package (VASP) [43,44]. The van der Waals (vdW) correction to the GGA functional was included by using the DFT-D2 method of Grimme [45]. The inherent underestimation of the band gap given by DFT within the inclusion of spin-orbit coupling (SOC) is corrected by using the Heyd-Scuseria-Ernzerhof (HSE) screened-nonlocal-exchange functional of the generalized Kohn-Sham scheme [46]. Analysis of the charge transfers in the structures was determined by the Bader technique [47].

The energy cutoff value for the plane-wave basis set was taken to be 500 eV. The total energy was minimized until the energy variation in successive steps became less than 10^{-5} eV in the structural relaxation and the convergence criterion for the Hellmann-Feynman forces was taken to be 10^{-4} eV/Å. The minimum energy was obtained by varying the lattice constant and the pressure was reduced below 1 kbar. $27 \times 27 \times 1$ Γ-centered k-point sampling is used for the primitive unit cell. The Gaussian broadening for the density of states calculation was taken to be 0.05. In order to investigate the effect of an external electric field, an electric field is applied in the direction normal to the plane of the heterobilayer. The binding energy per unit cell was calculated by using the following formula: $E_{\text{bind}} = E_{WS_2} + E_{Mg(OH)_2} - E_{\text{hetero}}$, where E_{WS_2} and $E_{Mg(OH)_2}$ denote the total energies of WS_2 and $Mg(OH)_2$ monolayers, respectively, while E_{hetero} denotes the total energy of the heterobilayer structure.

The dielectric function and the optical oscillator strength of the individual monolayers and the heterostructure were calculated by solving the Bethe-Salpeter equation (BSE) on top of single-shot GW (G_0W_0) calculation, which was performed over standard DFT calculations including SOC. During this process we used $15 \times 15 \times 1$Γ-centered k-point sampling. The cutoff for the response function was set to 200 eV. The number of bands used in our calculations is 320. The cutoff energy for the plane waves was chosen to be 400 eV. We included four (eight) valence and four (eight) conduction bands into the calculations for the dielectric function of individual monolayers (heterobilayers) in the BSE step.

In order to be certain that the calculated absorption spectra of the heterobilayer are converged with respect to k-point sampling and vacuum spacing between periodic layers, we performed convergence test calculations. These test calculations show that the optical gap of the heterobilayer is converged with $15 \times 15 \times 1$ k-point mesh and the absorption spectra does not change with further increasing of the vacuum spacing more than 11 Å. It is important to acknowledge that in some other 2D materials, the converged spectrum can be obtained by using $30 \times 30 \times 1$ k-point sampling and large vacuum spacing [48,49]. The main difference between the earlier reported calculations and our results is the inclusion of the truncated Coulomb interaction into the GW/BSE calculations. We are aware that the inclusion of the truncated Coulomb interaction is important in order to avoid long-range screening effects between the periodic layers; however, this is not supported by the version of VASP that we used for our calculations. This could be the reason why our absorption spectra converge with relatively less k-point mesh and vacuum spacing between periodic layers.

III. SINGLE-LAYER $Mg(OH)_2$ and WS_2

Monolayer $Mg(OH)_2$ consists of hydroxyl (OH) groups bonded to Mg atoms. As seen in Fig. 1, the layer of Mg atoms is sandwiched between the OH groups in which O and H atoms are strongly bonded to each other. The calculated lattice parameters for monolayer $Mg(OH)_2$ are $a = b = 3.13$ Å. The thickness of monolayer $Mg(OH)_2$ is 4.01 Å. The bond lengths of Mg-O and O-H bonds are calculated to be 2.09 Å and 0.96 Å, respectively. Bader charge analysis shows that ionic bond character is present in the $Mg(OH)_2$ monolayer. In the structure each H atom donates 0.6 e to the neighboring O atoms and each Mg donates 0.85 e per O atom.

Generic forms of monolayer structures of TMDs display honeycomb lattice symmetry with the 1H phase for the dichalcogenides of Mo and W atoms. The calculated lattice parameters for the 1H phase of the WS_2 monolayer are $a = b = 3.18$ Å, which is very close to that of the $Mg(OH)_2$ monolayer. The W-S bond length in WS_2 is calculated to be 2.42 Å. The thickness of the layer is 3.13 Å, which is thinner than the $Mg(OH)_2$ monolayer. In the monolayer WS_2 0.55 e of charge accumulation occurs from a W atom to each of the S atoms and the corresponding bonding character is covalent.

The calculated band structures within HSE06 correction are shown in Fig. 2. The $Mg(OH)_2$ monolayer is found to be a direct band-gap semiconductor with a band gap of 4.75 eV. Both the valence band maximum (VBM) and the conduction band minimum (CBM) reside at the Γ point in the Brillouin zone (BZ). The states in the VBM of the $Mg(OH)_2$ monolayer are composed of p_x and p_y orbitals of the O atoms.

Similar to the monolayer $Mg(OH)_2$, monolayer WS_2 is also a direct band-gap semiconductor but with a lower band gap of 2.30 eV. As in other TMDs, both the VBM and CBM of single-layer WS_2 lie at the K point in the BZ. As seen in Fig. 2(b), spin-orbit interaction at the VBM states is much stronger, since the states are composed of d_{x^2} and d_{z^2} orbitals of

TABLE I. The calculated ground-state properties of monolayer and their heterobilayer structures: structure, lattice parameters of primitive unit cell, a and b (see Fig. 1), the distance between the individual atoms contained in each monolayer d_{X-Y}, magnetic state, the total amount of charge received by the O or S atoms $\Delta\rho$, the binding energy per unit cell between the monolayer in the heterobilayer E_{bind}, the energy-band gap of the structure calculated within GGA (E_g^{GGA}), SOC (E_g^{SOC}), and HSE06 (E_g^{HSE}), and work function Φ determined from $Mg(OH)_2$ side.

	Geometry	a (Å)	b (Å)	$d_{\text{Mg-O}}$ (Å)	$d_{\text{O-H}}$ (Å)	$d_{\text{W-S}}$ (Å)	Magnetic state	$\Delta\rho$ (e)	E_{bind} (meV)	E_g^{GGA} (eV)	E_g^{SOC} (eV)	E_g^{HSE} (eV)	Φ (eV)
$Mg(OH)_2$	1T	3.13	3.13	2.09	0.96		NM	2.9		3.25	3.22	4.75	4.15
WS_2	1H	3.18	3.18			2.41	NM	1.1		1.86	1.54	2.30	5.29
Heterobilayer	1T	3.16	3.16	2.10	0.96	2.41	NM		147	1.05	0.97	2.24	4.34

W atoms. There is an energy splitting of 430 meV at the VBM which is much larger than that of the monolayer $Mg(OH)_2$, which is calculated to be 25 meV.

IV. HETEROBILAYER

The calculated lattice constants of $Mg(OH)_2$ and WS_2 monolayers are very close to each other and therefore it is possible to construct a heterostructure of these monolayers where we may assume a primitive unit cell containing eight atoms in total. We considered three different high-symmetry stacking configurations of the monolayers (see Fig. 3). We found that two of the stacking configurations have binding energies very close to each other, but the one with the W atoms residing on top of an interface OH group is the ground state with a binding energy of 147 meV. We also performed energy-band structure calculation for the stacking configuration given in Fig. 3(c). The energy-band structures of two configurations have exactly the same properties. Thus in this paper we studied only the electronic properties of the ground-state configuration [see Fig. 3(b)]. For the lowest energy stacking configuration the interlayer distance is calculated to be 2.09 Å and the individual atomic bond lengths remain the same as in their isolated layers. The analysis for the charge transfers between the individual layers demonstrates that there is no depletion from one layer to the other for all the stacking geometries shown in Fig. 3. This result is expected due to the weak vdW interaction between the individual layers.

As shown in Table I, the calculated energy-band structure for the heterobilayer displays a semiconducting character with an indirect band gap of 2.24 eV. As seen in Fig. 4, the VBM of the heterobilayer that originates from the $Mg(OH)_2$ layer lies at the Γ point while the CBM of the structure which arises from the WS_2 layer lies at the K point. The calculated energy-band diagram of the heterostructure also indicates the weak interlayer interaction. As seen in Fig. 4, the partial density of states (PDOS) indicates that the VBM of heterobilayer exclusively consists of p_x and p_y orbitals of the O atoms, while the CBM is characterized by the orbitals of W

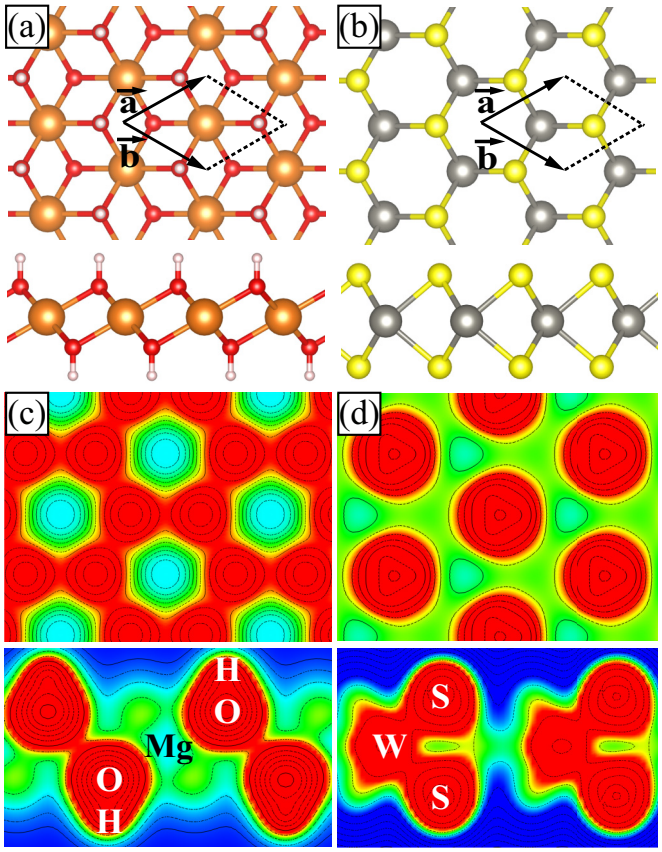

FIG. 1. Top and side view of monolayers of (a) $Mg(OH)_2$ and (b) WS_2. The charge distribution on the individual atoms are shown in top and side views of (c) $Mg(OH)_2$ and (d) WS_2. Increasing charge density is shown by a color scheme from blue to red with the formula $F(N) = 1 \times 1000^{N/\text{step}}$ where step size is taken to be 10 and N ranges from −1 to 2.

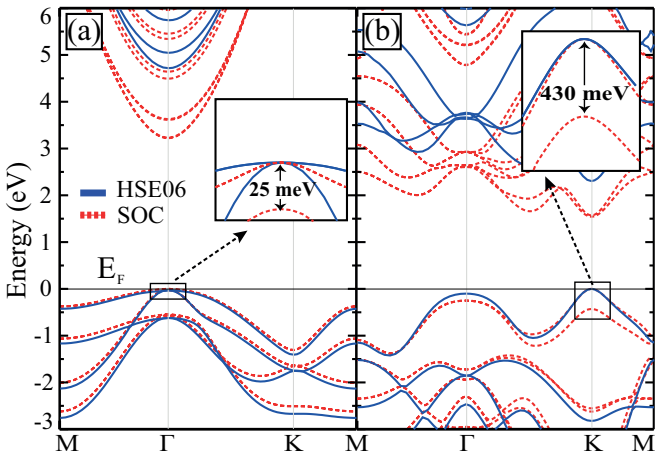

FIG. 2. Calculated energy-band structure of monolayer (a) $Mg(OH)_2$ and (b) WS_2. The Fermi energy (E_F) level is set to the valence band maximum.

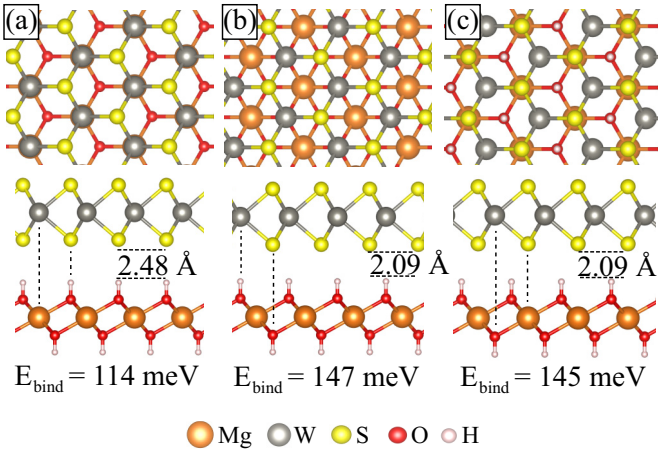

FIG. 3. Different possible stacking configurations for the heterobilayer structure: (a) W atom on top of Mg atom, (b) W atom on top of upper OH group, and (c) W atom on top of lower OH group.

and S atoms. This also demonstrates the type-II nature of the heterojunction: the two band edges originate from different individual layers and consequently, the excited electrons and holes are confined in different layers, which leads to the formation of spatially indirect excitons.

V. EFFECT OF EXTERNAL ELECTRIC FIELD

Applying an external electric field is one of the common methods to modify or tune the physical properties of materials. In the field of 2D materials, a perpendicular electric field can lead to doping and in the case of bilayers it can induce charge transfer between layers. Castro *et al.* reported that the electronic band gap of a graphene bilayer structure can be controlled externally by applying a gate bias. They showed that the band gap changes from zero to midinfrared energies for field values $\leqslant 1$ V/nm [50]. Chu *et al.* showed a continuous band-gap tuning in bilayer MoS_2 with applied gate voltage [51]. Here we present our results for the effect of a perpendicular electric field on the electronic and optical properties of the heterobilayer.

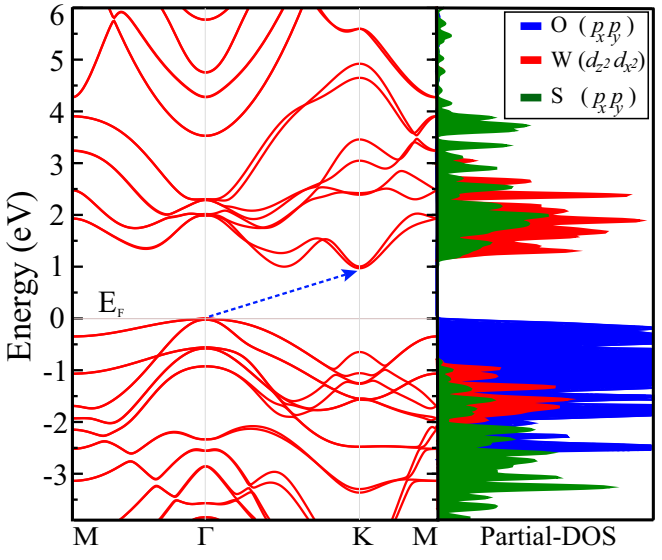

FIG. 4. The band structure (left) and the corresponding partial density of states (PDOS) (right) of the heterobilayer structure calculated within the SOC. The Fermi energy (E_F) level is set to the valence band maximum.

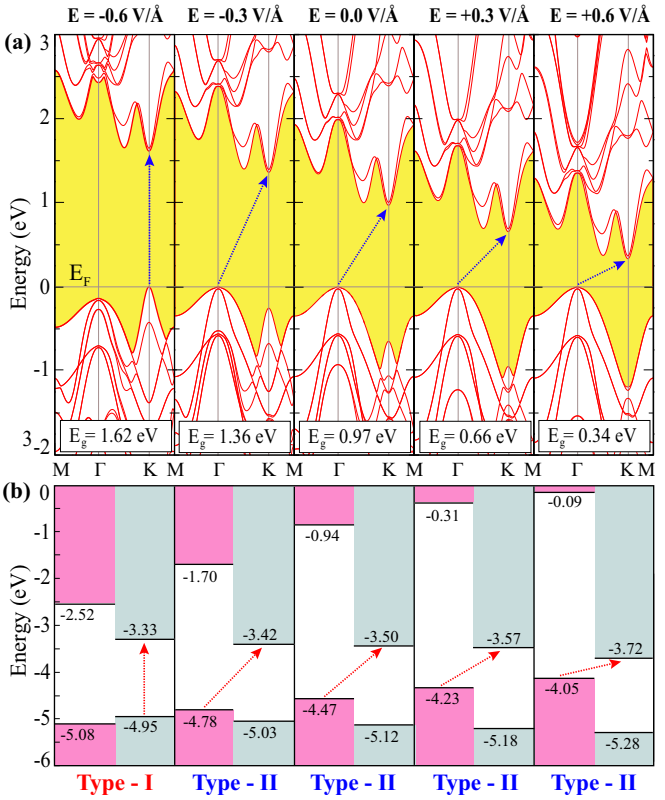

FIG. 5. (a) The effect of an external out-of-plane electric field on the band structure of the heterobilayer and (b) the corresponding band alignments (vacuum levels are set to zero). The band-gap regions are highlighted in yellow, while the CBM and VBM are highlighted in pink and gray for $Mg(OH)_2$ and WS_2, respectively.

As seen in Fig. 5(a), the heterostructure is an indirect band-gap semiconductor when there is no external electric field in which the VBM is at Γ but the CBM is at the K point. Applying a positive electric field decreases the band gap (from 0.97 eV to 0.34 eV for $E = +0.6$ V/Å). The reason for such decreasing band gap is the shift of the band edges at the Γ and the K points. Increasing the value of the positive electric field shifts the VBM of $Mg(OH)_2$ up in energy while it shifts the CBM of WS_2 down, resulting in a decrease of the energy gap. The indirect character of the energy gap is not affected by the field. However, changing the direction of the applied electric field widens the band gap and ultimately leads to an indirect-to-direct band-gap crossover as seen in Fig. 5(a).

When the strength of the electric field is -0.6 V/Å, it is clearly seen that both the VBM and CBM of the heterobilayer reside at the K high-symmetry point in the BZ. Thus a transition from staggered gap to a straddling gap (type-I heterojunction) occurred as shown in Fig. 5(b). In fact, the critical electric field value for which this indirect-to-direct band-gap crossover occurs is calculated to be 0.51 V/Å. At

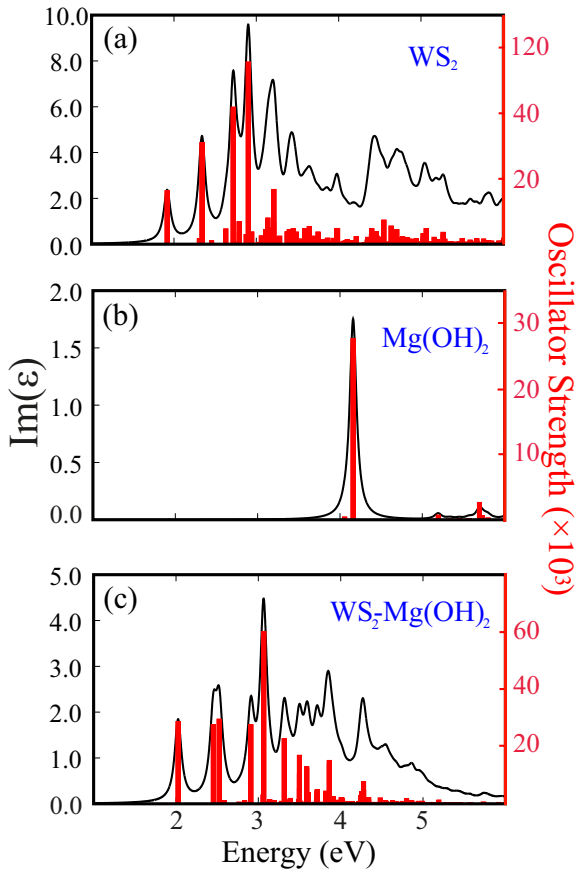

FIG. 6. Imaginary part of the dielectric function and the oscillator strength of the optical transitions (red bars) of (a) WS_2 monolayer, (b) $Mg(OH)_2$ monolayer, and (c) $WS_2-Mg(OH)_2$ heterostructure.

this critical value of the applied electric field, the valence band-edge energy of the bands at the Γ and K points becomes degenerate. As seen in Fig. 5(a), the bands at the valence band edge of the K point, which originate from the WS_2 layer, shift up while the bands at the Γ point which originate from the $Mg(OH)_2$ layer shift down when making the external electric field more negative. Due to these opposite shifts of the VBM of the individual layers [see Fig. 5(b)] a transition from indirect-to-direct gap is predicted at a certain value of the applied field. After the transition to type-I heterojunction, both types of charge carriers are confined to the WS_2 layer, which is desirable for applications in optoelectronic devices and for semiconductor laser applications. It is also important to point out that including quasiparticle energies might slightly change the band gap and the electric field value for which the indirect-to-direct band-gap crossover occurs. However, the overall tunability characteristic of the heterobilayer using the electric field would remain the same.

VI. OPTICAL PROPERTIES

In order to investigate the optical properties of the isolated monolayers and the heterostructure, we solved the BSE equation on top of G_0W_0 calculation. In Fig. 6 we show the imaginary part of the dielectric function and the oscillator strength of the optical transitions of WS_2 [Fig. 6(a)], $Mg(OH)_2$ [Fig. 6(b)], and $WS_2-Mg(OH)_2$ heterostructure [Fig. 6(c)].

The first two peaks at 1.917 and 2.309 eV in the optical spectrum of monolayer WS_2 [Fig. 6(a)] originate from the optical transitions at the K point in the BZ. The splitting (392 meV) of these two peaks is consistent with the splitting of the VBM bands at the K point due to the SOC effect (see Fig. 2). Our calculations show that the oscillator strength of the optical transitions of the WS_2 monolayer is an order of magnitude larger than that of the $Mg(OH)_2$ monolayer. The first two optical transitions for the monolayer $Mg(OH)_2$ [Fig. 6(b)] are split with a very small energy of 102 meV; this value is close to the value of the VBM splitting at the Γ point due to the SOC effect (Fig. 2). The exciton binding energy of WS_2 and $Mg(OH)_2$ is found to be 0.44 eV and 2.23 eV, respectively.

In Fig. 6(c) we show the imaginary part of the dielectric function and the oscillator strength of the optical transitions of the $WS_2-Mg(OH)_2$ heterostructure. As seen from the figure, the first two peaks in the optical spectrum originate from the WS_2 monolayer. The splitting of the first two peaks increases to 428 meV and their positions are blueshifted due to the interaction between the two monolayers. Although the oscillator strengths of the peaks from the $Mg(OH)_2$ monolayer are small, they can still be identified at around 4 eV in the optical spectrum. As seen from Fig. 6(c), the main optical transitions of the heterostructure originate from the intralayer recombinations of each monolayer. This is due to the low oscillator strength of the interlayer excitons.

As mentioned before, the $WS_2-Mg(OH)_2$ heterobilayer has a type-II alignment and it transforms into a type-I heterostructure under an external out-of-plane electric field

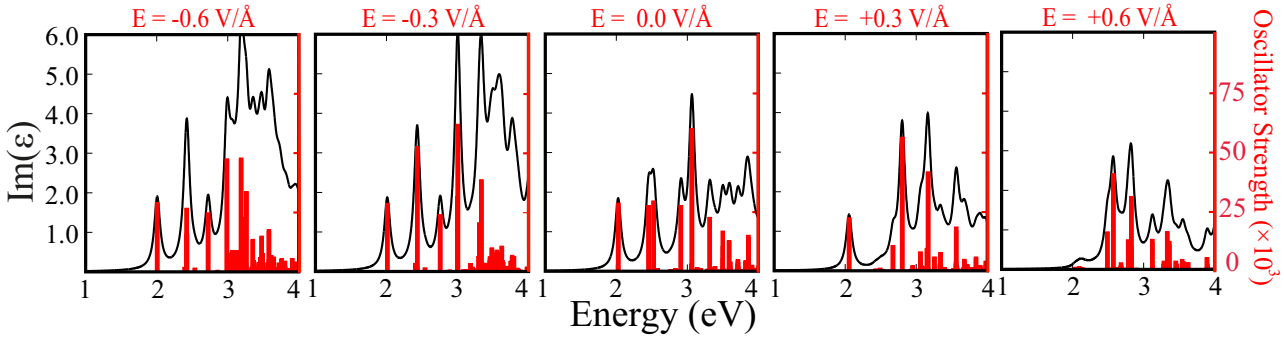

FIG. 7. Imaginary part of the dielectric function and the oscillator strength of the optical transitions (red bars) for different values of the perpendicular electric field.

of −0.51 V/Å. In order to investigate the variation in the optical properties of the heterobilayer under different electric field strengths, we calculated the dielectric function and the oscillator strength of the different optical transitions under out-of-plane electric fields of –0.6, –0.3, 0, 0.3, and 0.6 V/Å, which are shown in Fig. 7. Our calculations show that except from the 0.6 V/Å, the low-energy part of the absorption spectra of the heterobilayer is dominated by the intralayer exciton peaks from the WS_2 monolayer. For the 0.6 V/Å case, the oscillator strength of the exciton peaks around 2 eV are suppressed drastically.

VII. CONCLUSION

We investigated the structural, electronic, and optical properties of the monolayers $Mg(OH)_2$ and WS_2 and their heterobilayer structure. In addition, the effects of an applied out-of-plane electric field on the electronic and optical properties of the heterobilayer were investigated. We found that both $Mg(OH)_2$ and WS_2 are direct-gap semiconductors, while the $Mg(OH)_2-WS_2$ heterobilayer structure is an indirect-gap semiconductor. Our results demonstrated that both the band gap and the energy-band dispersion of the heterobilayer structure can be tuned by the application of an external perpendicular electric field. At an applied electric field of –0.51 V/Å, a transition from a staggered to a straddling gap heterojunction occurs which can be used for optoelectronic and semiconductor laser applications. In addition, by solving the Bethe-Salpeter equation on top of single-shot G_0W_0 calculations, we predict that the low-energy spectrum of the heterobilayer is dominated by the intralyer excitons of the WS_2 monolayer. It appears that heterobilayers of TMDs and AEHs may find applications in various nanoscale optoelectronic devices.

ACKNOWLEDGMENTS

This work was supported by the Flemish Science Foundation (FWO-Vl) and the Methusalem foundation of the Flemish government. Computational resources were provided by TUBITAK ULAKBIM, High Performance and Grid Computing Center (TR-Grid e-Infrastructure). H.S. is supported by a FWO Pegasus Long Marie Curie Fellowship. H.S. and R.T.S. acknowledge support from TUBITAK through Project No. 114F397. H.S. acknowledges support from Bilim Akademisi – The Science Academy, Turkey, under the BAGEP program.

[1] K. S. Novoselov, A. K. Geim, S. V. Morozov, D. Jiang, Y. Zhang, S. V. Dubonos, I. V. Grigorieva, and A. A. Firsov, Science **306**, 666 (2004).
[2] K. S. Novoselov, A. K. Geim, S. V. Morozov, D. Jiang, M. I. Katsnelson, I. V. Grigorieva, S. V. Dubonos, and A. A. Firsov, Nature (London) **438**, 197 (2005).
[3] K. S. Novoselov, D. Jiang, F. Schedin, T. Booth, V. V. Khotkevich, S. Morozov, and A. K. Geim, Proc. Natl. Acad. Sci. U. S. A. **102**, 10451 (2005).
[4] H. Sahin, S. Cahangirov, M. Topsakal, E. Bekaroglu, E. Akturk, R. T. Senger, and S. Ciraci, Phys. Rev. B **80**, 155453 (2009).
[5] R. A. Gordon, D. Yang, E. D. Crozier, D. T. Jiang, and R. F. Frindt, Phys. Rev. B **65**, 125407 (2002).
[6] Q. H. Wang, K. K. Zadeh, A. Kis, J. N. Coleman, and M. S. Strano, Nat. Nanotechnol. **7**, 699 (2012).
[7] B. Radisavljevic, A. Radenovic, J. Brivio, V. Giacometti, and A. Kis, Nat. Nanotechnol. **6**, 147 (2011).
[8] X. Lu, M. I. B. Utama, J. Lin, X. Gong, J. Zhang, Y. Zhao, S. T. Pantelides, J. Wang, Z. Dong, Z. Liu, W. Zhou, and Q. Xiong, Nano Lett. **14**, 2419 (2014).
[9] H. S. S. R. Matte, A. Gomathi, A. K. Manna, D. J. Late, R. Datta, S. K. Pati, and C. N. R. Rao, Angew. Chem., Int. Ed. **49**, 4059 (2010).
[10] S. Tongay, H. Sahin, C. Ko, A. Luce, W. Fan, K. Liu, J. Zhou, Y. S. Huang, C. H. Ho, J. Y. Yan, D. F. Ogletree, S. Aloni, J. Ji, S. S. Li, J. B. Li, F. M. Peeters, and J. Q. Wu, Nat. Commun. **5**, 3252 (2014).
[11] D. Wolverson, S. Crampin, A. S. Kazemi, A. Ilie, and S. J. Bending, ACS Nano **8**, 11154 (2014).
[12] H. Sahin, E. Torun, C. Bacaksiz, S. Horzum, J. Kang, R. T. Senger, and F. M. Peeters, WIRES **6**, 351 (2016).
[13] J. Wilson and A. Yoffe, Adv. Phys. **18**, 193 (1969).
[14] C. Ataca, H. Sahin, and S. Ciraci, J. Phys. Chem. C **116**, 8983 (2012).
[15] A. C. Gomez, M. Poot, G. A. Steele, H. S. J. van der Zant, N. Agrait, and G. R. Bollinger, Adv. Mater. **24**, 772 (2012).
[16] H. Li, Z. Yin, Q. He, H. Li, X. Huang, G. Lu, D. W. H. Fam, A. I. Y. Tok, Q. Zhang, and H. Zhang, Small **8**, 63 (2012).
[17] I. Popov, G. Seifert, and D. Tomanek, Phys. Rev. Lett. **108**, 156802 (2012).
[18] G. Eda, H. Yamaguchi, D. Voiry, T. Fujita, and M. Chen, Nano Lett. **11**, 5111 (2011).
[19] K. F. Mak, C. Lee, J. Hone, J. Shan, and T. F. Heinz, Phys. Rev. Lett. **105**, 136805 (2010).
[20] Z. Yin, H. Li, H. Li, L. Jiang, Y. Shi, Y. Sun, G. Lu, Q. Zhang, X. Chen, and H. Zhang, ACS Nano **6**, 74 (2012).
[21] T. Drescher, F. Niefind, W. Bensch, and W. Grunert, J. Am. Chem. Soc. **134**, 18896 (2012).
[22] A. M. Seayad and D. M. Antonelli, Adv. Mater. **16**, 765 (2004).
[23] K. Chang and W. X. Chen, ACS Nano **5**, 4720 (2011).
[24] T. Boker, R. Severin, A. Muller, C. Janowitz, R. Manzke, D. Voss, P. Kruger, A. Mazur, and J. Pollmann, Phys. Rev. B **64**, 235305 (2001).
[25] A. Klein, S. Tiefenbacher, V. Eyert, C. Pettenkofer, and W. Jaegermann, Phys. Rev. B **64**, 205416 (2001).
[26] M. Thomalla and H. Tributsch, J. Phys. Chem. B **110**, 12167 (2006).
[27] A. Ramasubramaniam, Phys. Rev. B **86**, 115409 (2012).
[28] H. Shi, H. Pan, Y. W. Zhang, and B. I. Yakobson, Phys. Rev. B **87**, 155304 (2013).
[29] K. F. Mak, K. He, C. Lee, G. H. Lee, J. Hone, T. F. Heinz, and J. T. Shan, Nat. Mater. **12**, 207 (2013).
[30] C. Estrela, F. C. Pimenta, I. Y. Ito, and L. L. Bammann, J. Endod. **24**, 15 (1998).

[31] E. Ghali, W. Dietzel, and K. U. Kainer, J. Mater. Eng. Perform. **13**, 7 (2004).
[32] Q. Cao, F. Huang, Z. Zhuang, and Z. Lin, Nanoscale **4**, 2423 (2012).
[33] E. Torun, H. Sahin, and F. M. Peeters, Phys. Rev. B **93**, 075111 (2016).
[34] L. Desgranges, G. Calvarin, and G. Chevrier, Acta Crystallogr., Sect. B: Struct. Sci. **52**, 82 (1996).
[35] M. Catti, G. Ferraris, S. Hull, and A. Pavese, Phys. Chem. Miner. **22**, 200 (1995).
[36] W. R. Busing and H. A. Levy, J. Chem. Phys. **26**, 563 (1957).
[37] T. Murakami, T. Honjo, and T. Kuji, Mater. Trans. **52**, 1689 (2011).
[38] M. Chiba, D. Endo, K. Haruta, H. Kimura, and H. Kiyota, MRS Proc. **1414**, 197 (2013).
[39] C. H. Huang, Y. L. Jan, and W. C. Lee, J. Electrochem. Soc. **158**, 879 (2011).
[40] A. Suslu, K. Wu, H. Sahin, B. Chen, S. Yang, H. Cai, T. Aoki, S. Horzum, J. Kang, F. M. Peeters, and S. Tongay, Sci. Rep. **6**, 20525 (2016).
[41] J. P. Perdew, K. Burke, and M. Ernzerhof, Phys. Rev. Lett. **77**, 3865 (1996).
[42] J. P. Perdew, K. Burke, and M. Ernzerhof, Phys. Rev. Lett. **78**, 1396 (1997).
[43] G. Kresse and J. Hafner, Phys. Rev. B **47**, 558 (1993).
[44] G. Kresse and J. Hafner, Phys. Rev. B **49**, 14251 (1994).
[45] S. J. Grimme, J. Comput. Chem. **27**, 1787 (2006).
[46] J. Heyd, G. E. Scuseria, and M. Ernzerhof, J. Chem. Phys. **118**, 8207 (2003).
[47] G. Henkelman, A. Arnaldsson, and H. Jonsson, Comput. Mater. Sci. **36**, 354 (2006).
[48] F. Hüser, T. Olsen, and K. S. Thygesen, Phys. Rev. B **88**, 245309 (2013).
[49] D. Y. Qiu, F. H. da Jornada, and S. G. Louie, Phys. Rev. B **93**, 235435 (2016).
[50] E. V. Castro, K. S. Novoselov, S. V. Morozov, N. M. R. Peres, J. M. B. Lopes dos Santos, J. Nilsson, F. Guinea, A. K. Geim, and A. H. CastroNeto, Phys. Rev. Lett. **99**, 216802 (2007).
[51] T. Chu, H. Ilatikhameneh, G. Klimeck, R. Rahman, and Z. Chen, Nano Lett. **15**, 8000 (2015).